ISSN 8755-6839

SCIENCE OF **TSUNAMI HAZARDS**

Journal of Tsunami Society International

Volume 40 Number 4 2021

RUPTURE IMAGING FOR THE 30 OCTOBER TSUNAMIGENIC EARTHQUAKE IN THE EASTERN AEGEAN SEA

Madlazim, Muhammad Nurul Fahmi, Arie Realita, Dyah Permata Sari

Universitas Negeri Surabaya, Indonesia

ABSTRACT

On 30 October 2020, an earthquake with a moment magnitude Mw=7.0 occurred in the Aegean Sea close to the coasts of Turkey and of the Greek Island of Samos. The earthquake generated a local tsunami in the area, which had maximum amplitude of 2 meters, and inundation in certain coastal region of up to 155 times the run-up height. The present study provides a measure of the rupture dynamics of this tsunamigenic earthquake and provides the parameters of its rupture velocity, as well as the direction and length of the rupture by using beam forming and Multiple Signal Classification Back Projection (MUSICBP) techniques. In this present study we used 189 AK array stations and 153 European (EU) networks stations. The area of high frequency (HF) radiators extends almost bilaterally for more than 64 km along the rupture dynamics, with almost all ruptures having westward directivity. However, there was also an eastward rupture with high energy and low velocity. The timing of the HF radiators seen by both arrays were plotted against their epicenter distance slope 1 of the blue lines, which indicated rupture speeds of 1.9 km/s (slow), and the slope 2 of the yellow lines indicated very fast rupture speeds of 5 km/s, while the slope 3 of the purple lines indicated average rupture speeds of 3.3 km/s (regular).

Keywords: *Rupture imaging, back projection, rupture velocity, tsunami run-up*

1. INTRODUCTION

Seismologists have identified different types of earthquakes, which are mainly classified according to their duration and frequency during the process of releasing their energy. Several types of large slow earthquakes or non-regular, slow slip events (SSE), episodic and tremor slip earthquakes (ETS), silent earthquakes, and tsunamigeni earthquakes have been detected and observed in certain zones around the world. On October 30th, 2020, there was a magnitude 7.0 earthquake in the Aegean Sea, was followed by a tsunami with a maximum amplitude of 2 meters and 155 times run-up (National Geophysical Data Center / World Data Service: NCEI/WDS Global Historical Tsunami Database. NOAA National Centers for Environmental Information.doi: 10.7289/V5PN93H7).

The tsunami was generated in the Eastern Aegean Sea is interesting to study because such high tsunami wave run-up rarely occurs with earthquakes with a moment magnitude Mw = 7.0, particularly when the earthquake occurs on a normal fault, as this type of of this particular earthquake (Dogan, GG, et al., 2021). Riquelme, S. et al., (2018) have found a relationship between the number of tsunami run-up and the earthquake rupture velocity. They have measured the amplification due to very slow release moment. They found that this rupture velocity parameter plays a key role in run-up amplification. The smaller the earthquake rupture velocity, the greater the number of tsunami run-up. The rupture velocity (Vr) is related to the rupture duration (T) and the rupture length (L) of the earthquake as stated in the equation Vr=(L)/T. This means that the smaller the rupture velocity, the greater the duration of the rupture. Earthquakes that have a rupture duration greater than 50 seconds have the potential to cause a tsunami (Lomax and Micellini, 2011); Madlazim et al., 2021, 2020, 2017, 2013). Ma (2012) explains the possibility of a tsunami from a slow earthquake that changes the pore pressure when an earthquake occurs. In his work, simulations of dynamic pore pressure changes show that as dynamic pore pressures increase, due to upward propagation of rupture causes extensive yielding within the wedge, increase seafloor displacement. Ma and Hirakawa (2013) also suggested that due to dynamic wedge failure, it is possible to generate scenarios with more deformation in the trench, slower rupture rates and less seismic moments in the fault plane. Based on this relationship, it can be assumed that an earthquake that has a small rupture velocity or a slow earthquake has the potential to generate a tsunami. Riquelme1 and Fuentes (2021) have calculated the relationship between tsunami magnitude, rupture velocity and amplitude and the efficiency of very slow tsunamigenic earthquakes. The slow earthquake rupture velocity (< 2 km/s) is most likely to generate a tsunami.

Low velocity of earthquake rupture can be caused by a medium, which includes sediment. The North Aegean Sea and its surroundings are areas that have accumulated Tertiary sediments from the Eocene to the present. During this sedimentation, the general pattern of the basin appears to have been preserved. Overall, the basin has become more abundant in the south through time, and the NW trending basin has become more prominent (Ioannis K. Koukouvelas1 and Atilla Aydin (2002). On the basis of stratigraphy and structural data, it is suggested that the North Aegean Trench began to form during the Miocene. The basin analysis in the NW Turkey shows that the North Anatolian Fault

spreads westward to the Sea. The composition of the terrigenous fraction in the sedimentary sea reflects the geology of the surrounding landmass, as well as the dominant sedimentary processes. The terrigenous fraction in the Aegean Sea has its sources in the Aegean islands and medium-sized river drainage basins flowing into the Aegean Sea (İŞLER, EB, et al., 2016).

This present study focuses on measuring the rupture dynamics of the Mw=7.0 earthquake that generated a tsunami on October 30th, 2020 in the Eastern Aegean Sea, including the parameters of rupture velocity, direction, and length.

2. METHOD

Back projection of high frequency seismic waves (HF) recorded by dense arrays (Fletcher et al., 2006; Ishii et al., 2005) provides unique insights into earthquake rupture processes that complement the limited sources of traditional inversion. The back projection of the array aims to trace the area of the source that produces the highest frequency of the strongest radiation, only based on the phase and coherence of the seismic array signal. This provides a strong constraint on the spatiotemporal evolution of earthquake ruptures, without relying on the assumed Green function or on the restrictive kinematic parameterization of the rupture. We used the back projection method of P-wave seismic waveforms recorded by two arrays at teleseismic distances, AK array and the EU network (Fig. 1). We causally filtered the waveform from 0.5 to 1 Hz, the highest band where the coherent arrival initials are to be strongly aligned. We then applied two different array processing techniques: beam forming technique and Multiple Signal Classification Back Projection (MUSICBP) (Meng, L. et al., 2011; Bao, H., et al., 2019), a resolution technique designed to complete close-range simultaneous sources; and correlation stacking (Fletcher et al., 2006), a technique known to increase robustness in the presence of scattering. Our results based on these two techniques are mutually consistent. To create earthquake rupture imaging,

A back-projection method that uses teleseismic earthquake seismogram data is adopted, using a series of linear equations that relate the observed data to the model:

$$\mathbf{d = Gm} \tag{1}$$

Where d is teleseismic seismogram data from earthquakes with a moment magnitude > 6.5, “G” is Green's function, which is a synthetic seismogram calculated using a certain earth model, and “m” is the model, which is a slip function for each earthquake rupture. Conventional notation “d” is a data vector, “m” is a model vector, and “G” is a linear operator that predicts data from the model. The goal in geophysical inverse problems is to estimate “m” from observations, “d”. Assuming there are more data points than model points, the standard way to solve this problem is to define the residual vector, **r = d - Gm**, and find m that minimizes **r • r**. This is a least squares solution and it can be shown that:

$$m = (\mathbf{G}^{\mathbf{T}}\mathbf{G})^{-1}\mathbf{G}^{\mathbf{T}}\mathbf{d} \tag{2}$$

However, the $\mathbf{G}^T\mathbf{G}$ often is single or unconditioned, or maybe too big to flip. What can be done in these cases? The simplest and most crude way to proceed is to make the following estimation.

$$(\mathbf{G}^T\mathbf{G})^{-1} \approx \mathbf{I} \quad (3)$$

in this case we can estimate the model as

$$\mathbf{m} \approx \mathbf{G}^T\mathbf{d} \quad (4)$$

The GT transposition matrix is an adjoin or back-projection operator. Each model point is constructed as a weighted sum of the data points it affects. Could such a crude approach do any good? It is easy to think of examples where (3) invalid at all. However, in real geophysical problems, it is surprising how often this method works, especially if the scaling factor is allowed to bring the data and the model predicted data into better agreement, that is, assuming $(GT\ G)^{-1} \approx I$, with λ being a constant. Indeed, it is sometimes observed that an adjoint (back-projection) performs better than a formal inverse because it is more tolerant of imperfections in the data.

In seismology, the available seismogram data is usually a set of seismograms. In source inversion, we usually assume that the structure of the Earth's velocity is known and we solve for the location and timing of the seismic wave radiator (e.g. solving the slip model). In reflection seismology, we usually assume that the location and time of the source are known and we solve for the location of the reflector that cause the observed arrival. In each case, model estimation at each model point are obtained by finding the time in the seismogram at which model changes will affect the seismogram. Summing or stacking the seismogram values at these points obtains the model estimation of the back-projection. The main thing to calculate is the travel time between the model point and each recording station. This provides the time shift needed to find the time in each seismogram that is sensitive to model disturbance.

The data used in this study are earthquake seismogram data recorded by AK array, and EU network stations (Fig. 2). The following is a map of the earthquake event on October 30th, 2020 that occurred in the Aegean Sea, Turkey and the stations of the 2 Arrays (Fig. 1).

2A. Back Projection App for the 30 October 2020 Earthquake

We used beam forming and Multiple Signal Classification Back Projection (MUSICBP) techniques from Meng, L. et al (2011) and Bao, H., et al (2019). In this study, the focus is on estimating the imaging rupture of the earthquake that occurred in the Aegean, Turkey on October 30th, 2020 using the Back Projection method. We used 189 AK array stations and 153 EU networks stations (Fig. 1). The data from the two locations are in the form of earthquake seismograms in SAC format recorded by AK array, and EU networks (Fig. 2) and downloaded from IRIS DMC via the following link http://ds.iris.edu/wilber3/find_stations/11331986.

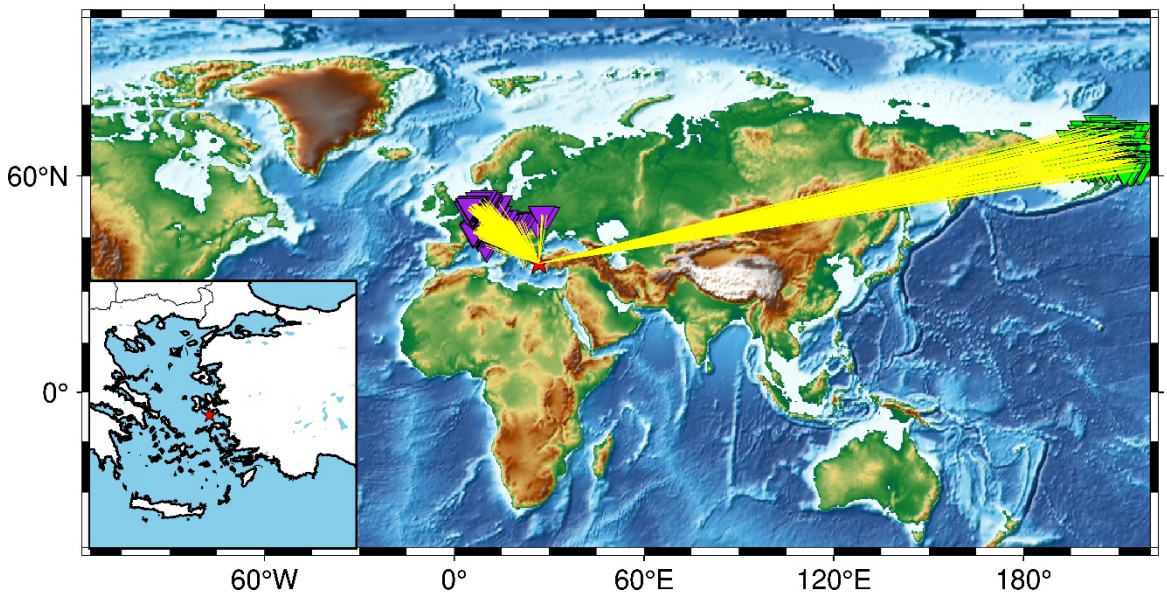

Figure 1. Epicenter of 30-10-2020 Aegean Sea, Turkey Earthquake (red star) and of EU network stations (group of purple triangles) and AK array (group of green triangles) distribution.

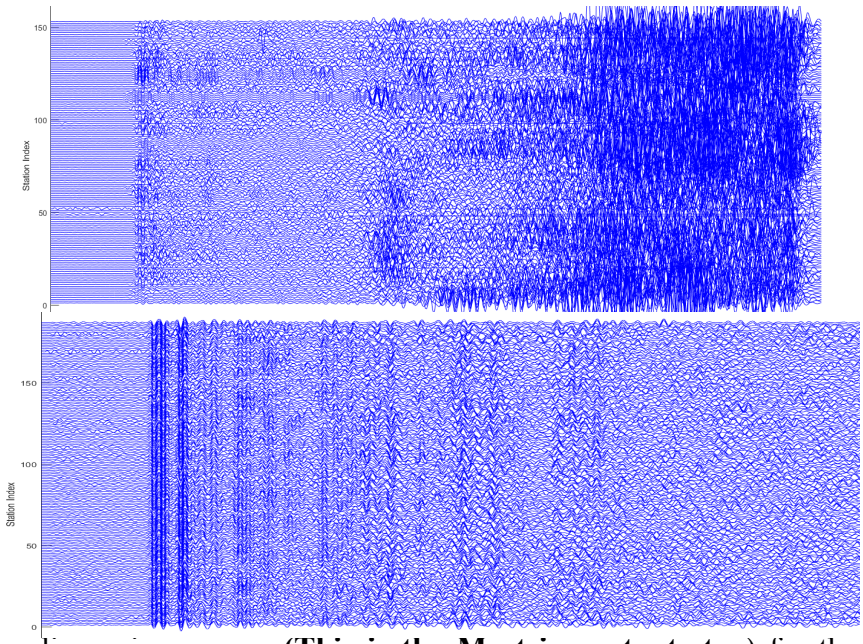

Figure 2. The align seismograms **(This is the Most important step)** for the AK array stations and EU network. The settings are suitable to align any first P arrival recorded at teleseismic distance. The top figure is seismograms from 153 stations of EU_network and bottom figure is seismograms from 189 stations of AK array.

3. RESULTS AND DISCUSSION

3A. High Resolution Array Analysis Using AK Array and European (EU) Network

Figure 3 shows the location of the strongest HF radiation region in a sliding window that is 25 seconds long. Secondary sources are often seen in our back projection images, for example between 26 and 50 seconds. However, our focus here is on first-order features that we can reliably identify by tracking the most coherent phases within each time window. The area of HF radiation extends almost bilaterally for more than 100 km along the rupture dynamics, almost all ruptures are westward, but there is an eastward rupture with high energy and low velocity (Fig. 3). It bridges the rupture area of several historic earthquakes in the Eastern Aegean Sea. The HF rupture is mostly westward from the hypocenter, and partially landward (Dogan, G.G., Yalciner, A.C., Yuksel, Y. et al., 2021). This ground-directed rupture dynamic has the highest energy (Fig. 4 left panel). It is very likely that this caused the enormous energy amplification that triggered the tsunami.

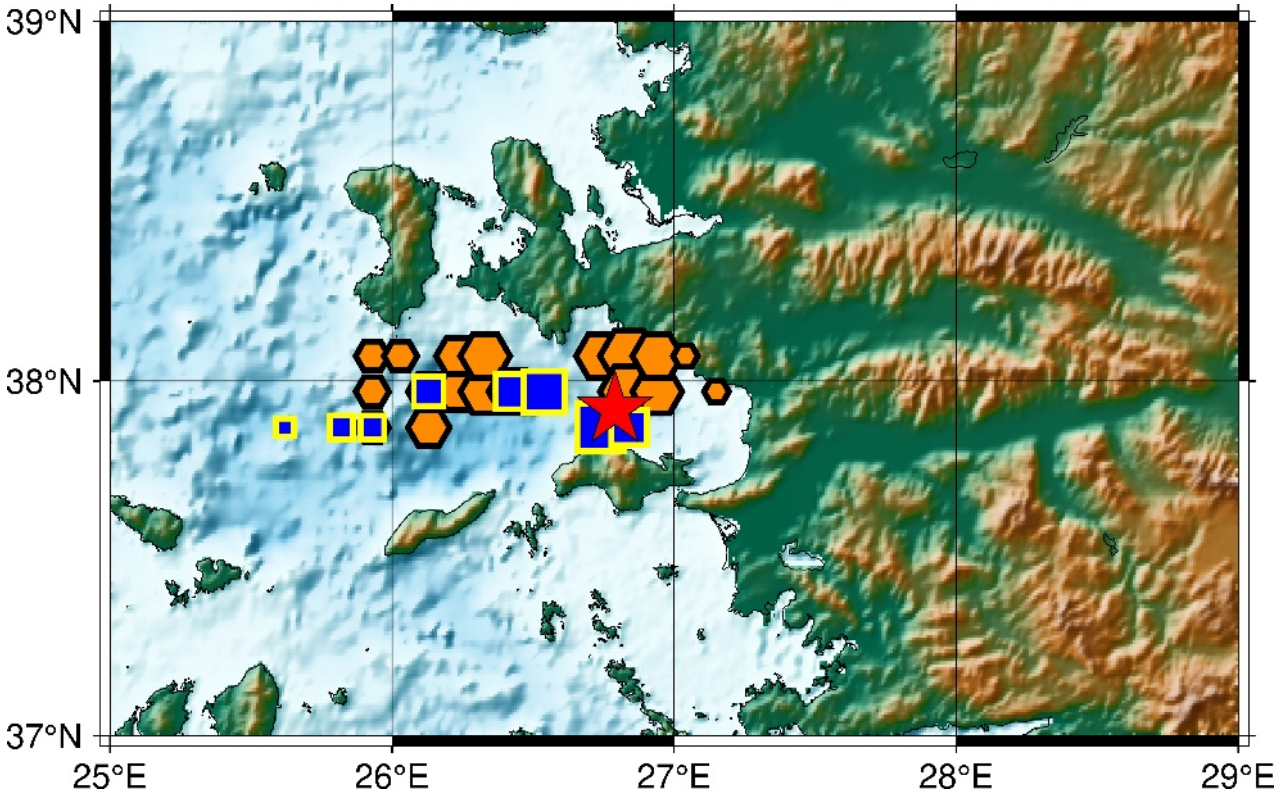

Figure 3. The Aegean Sea, Turkey earthquake imaged by the AK array and EU network. Location of the strongest high frequency radiators of the earthquake, seen by the AK array (blue squares) and by the EU network (brown polygons). The size indicate of relative amplitude of the energy. The red star is the epicenter of the earthquake.

3B. The Spatiotemporal Evolution of the Turkey Earthquake

In this study we used EU network and AK array stations. We have tried using AU array as well, but when we used AU array for the earthquake that occurred in the Aegean Sea on October 30th, 2020 an error occurred, so we decided to only used the AK array and EU networks. The result of this study is the time vs. relative amplitude of earthquake power (Fig. 4-left panel), which shows the temporal evolution of normalized amplitudes estimated at the AK array (blue) and at the European network (red). The numbers in circles mark the two phases with distinct rupture behavior. The timing of the high frequency radiators seen by both arrays are plotted against their epicenter distance, slope1 of the blue lines indicate rupture velocity of 1.9 km/s (slow), the slope2 of the yellow lines indicate very fast rupture velocity of 5 km/s, and the slope3 of the purple lines indicate average rupture velocity of 3.3 km/s (regular). For reference, the local crust S wave velocity is 3.42 to 4.5 km/s (Takahashi et al., 2004).

The length of the earthquake rupture can be estimated from Figure 4, which is about 64 km (Fig. 4-right panel). The spatiotemporal evolution of the strongest high frequency (HF) radiation is shown in Figure 4 right panel. Continuous HF Radiation energy was reliably imaged by our array back projection during the first 25 seconds of rupture (Fig 4 left panel). The overall size of HF rupture during this period of 0 to 10 seconds on average shows a low rupture velocity (1.9 km/s) along the 15 km rupture, which supports the higher tsunami run-up caused by this earthquake. Riquelme, S. et al., (2018) have found a relationship between the number of tsunami run-up and the earthquake rupture velocity. They have measured the amplification due to very slow release moment. They found that this rupture velocity parameter plays a key role in run-up amplification. The smaller the earthquake rupture velocity, the greater the number of tsunami run-up. Madlazim et al (2021a; 2021b, 2020, 2017, 2013) and Lomax and Michelini (2011) have also found that a strong indicator of a tsunami is the duration of an earthquake rupture that is more than 50 seconds. For rupture dynamics 11 seconds to 25 seconds the average shows a very high rupture velocity (5 km/s) along 50 km.

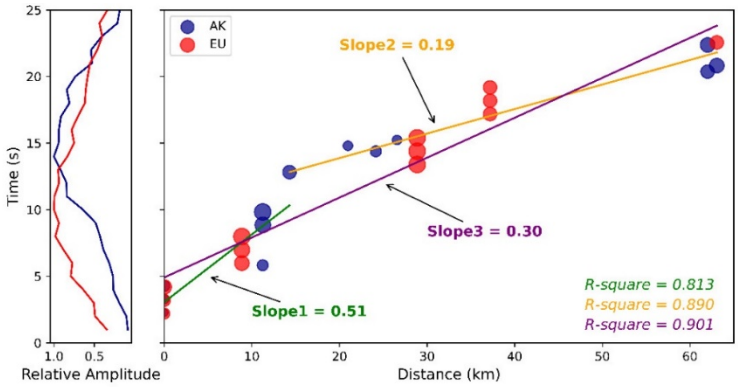

Figure 4. Rupture time versus epicenter distance. The timing of the high frequency radiators seen by both arrays is plotted against their epicenter distance. The color denotes AK array and EU network with respect to the epicenter and their relative amplitude normalized by the maximum amplitude during the event.

4. CONCLUSIONS

We have carried out a rupture imaging study for the earthquake that occurred in the Eastern Aegean Sea on October 30th, 2020. We used beam forming and Multiple Signal Classification Back Projection (MUSICBP) techniques. We found that the area of HF radiation extends almost bilaterally for more than 64 km along the rupture dynamics, and almost all of the ruptures are westward, but there is an eastward rupture with high energy and low velocity. The timing of the high frequency radiators seen by both arrays are plotted against their epicenter distance, slope 1 of the blue lines indicate rupture velocity of 1.9 km/s (slow), the slope 2 of the yellow lines indicate very fast rupture velocity of 5 km/s, and the slope 3 of the purple lines indicate average rupture velocity of 3.3 km/s (regular).

ACKNOWLEDGEMENTS

Our thanks go to Meng, L. and Bao, H. for allowing the use of the MUSICBP software for this research. We also thank IRIS DMC for allowing researchers to download earthquake data via the following link http://ds.iris.edu/wilber3/find_stations/11331986

REFERENCES

Bao, H., Ampuero, J. P., Meng, L., Fielding, E. J., Liang, C., Milliner, C. W., ... & Huang, H. (2019). Early and persistent supershear rupture of the 2018 magnitude 7.5 Palu earthquake. Nature Geoscience, 12(3), 200-205.

Fletcher, J. B., P. Spudich, and L. M. Baker (2006), Rupture propagation of the 2004 Parkfield, California, earthquake from observations at the UPSAR, Bull. Seismol. Soc. Am., 96(4B), S129–S142, doi:10.1785/ 0120050812.

Dogan, G.G., Yalciner, A.C., Yuksel, Y. *et al.* The 30 October 2020 Aegean Sea Tsunami: Post-Event Field Survey Along Turkish Coast. *Pure Appl. Geophys.* **178,** 785–812 (2021). https://doi.org/10.1007/s00024-021-02693-3

Ishii, M., P. M. Shearer, H. Houston, and J. E. Vidale (2005), Extent, duration and speed of the 2004 Sumatra‐Andaman earthquake imaged by the Hi‐Net array, Nature, 435(7044), 933–936

İŞLER, E. B., Ali Engin AKSU*, Richard Nicholas HISCOTT. 2016. Geochemistry of Aegean Sea sediments: implications for surface- and bottom-water conditions during sapropel deposition since MIS 5. *Turkish J Earth Sci* (2016) 25: 103-125©TÜBİTAK. doi:10.3906/yer-1501-35.

Koukouvelas Ioannis K., and Atilla Aydin. 2002. Fault structure and related basins of the North Aegean Sea and its surrounding. *TECTONICS*, VOL. 21, NO. 5, 1046, doi:10.1029/2001TC901037, 2002.

Lomax A, Michelini A (2011). Tsunami early warning using earthquake rupture duration and P-wave dominant period: the importance of length and depth of faulting. Geophysical Journal International 185(1): 283–291. https://doi.org/10.1111/j.1365-246X.2010.04916.x

Madlazim, Eko Hariyono, Muhammad Nurul Fahmi, Dyah Permata Sari. (2021a). Tsunami faulting model analysis for the 30 October 2020 normal earthquake. *Science of Tsunami Hazards*, accepted.

Madlazim, Prastowo T, Fahmi MN, Sari DP, Melianda E, Koesoema S. (2021b). Tsunamis from strike-slip and normal earthquakes and its relation with the product of dominant period and duration more than 50 seconds of earthquake P-wave. *Science of Tsunami Hazards*. 2021, 40(2), pp. 101–113

Madlazim Prastowo T, Fahmi MN (2020). Estimation of rupture directivity, CMT and earthquake tsunami parameters and their correlation with the main source of the first tsunami wave, September 28, 2018. *Science of tsunami hazards* 39(4): 228–242.

Madlazim (2017). Use of The Joko Tingkir Software for Rapid Determination of Tsunami Faulting Parameters Resulting From the Mw-7.8 Earthquake of March 2, 2016, in Southern Sumatra. *Science of Tsunami Hazards* 36(1): 41–48.

Madlazim (2013). Assessment of tsunami generation potential through rapid analysis of seismic parameters: Case study: Comparison of the Sumatra Earthquakes of 6 April and 25 October 2010. *Science of Tsunami Hazards* 32(1): 29-38.

Ma, S., and E. T. Hirakawa (2013), Dynamic wedge failure reveals anomalous energy radiation of shallow subduction earthquakes, *Earth Planet*. Sci. Lett., 375, 113 - 122, doi: 10.1016/j.epsl.2013.05.016.

Meng, L., A. Inbal, and J.-P. Ampuero. 2011. "A window into the complexity of the dynamic rupture of the 2011 Mw 9 Tohoku-Oki earthquake", Geophys. Res. Lett., 38, L00G07, doi:10.1029/2011GL048118.

Riquelme, S. , Fuentes, M. Campos, J., A. Schwarze, H. 2018**.** Implications on Tsunami Run-up due to Slow Ruptures Velocities. *American Geophysical Union*, Fall Meeting.

Sebastián Riquelme, Mauricio Fuentes; Tsunami Efficiency Due to Very Slow Earthquakes. *Seismological Research Letters* 2021;; 92 (5): 2998–3006. doi: https://doi.org/10.1785/0220200198.

Takahashi, N., S. Kodaira, T. Tsuru, J. O. Park, Y. Kaneda, K. Suyehiro, H. Kinoshita, S. Abe, M. Nishino, and R. Hino (2004), Seismic structure and seismogenesis off Sanriku region, northeastern Japan, Geophys. J. Int., 159(1), 129–145, doi:10.1111/j.1365-246X.2004.02350.x.

Kiser, E., & Ishii, M. (2017). Back-projection imaging of earthquakes. Annual Review of Earth and Planetary Sciences, 45, 271-299.